An exact approach for radius of curvature measurement in a calibration test sphere

Jaime M. JALIFE-CHAVIRA*, Gerardo TRUJILLO-SCHIAFFINO,
Paloma G. MENDOZA-VILLEGAS, Didia P. SALAS-PEIMBERT,
Marcelino ANGUIANO-MORALES, Luis F. CORRAL-MARTÍNEZ,
Edgar ZENDEJAS-HERNÁNDEZ

Tecnológico Nacional de México/Instituto Tecnológico de Chihuahua,
División de Estudios de Postgrado e Investigación,
Av. Tecnológico #2909 Chihuahua Chih., México, C.P. 31310

*Corresponding author: jmjalife@itchihuahua.edu.mx

In this paper we present a technique to measure the radius of curvature of a test sphere based on the relation between acquired images of a circular cosine fringe pattern and size of virtual image formed on the calibration test surface. Radius of curvature is calculated with the exact equation proposed, using the parameters of the optical setup. Fringe pattern evaluation was performed by locating extrema indices. The mathematical formulation as well as the experimental setup and results are presented. After applying a linear fit algorithm to the data as a method of compensation, obtained results show an error within the tolerance established by the ISO 10343 specifications.

Keywords: keratometry, radius of curvature, diopters, cosine fringe pattern, film.

1. Introduction

Human cornea is responsible for more than 70% of the total eye's refractive power [1], what makes it a vital anatomical structure to carry out the vision process. A correct image formation of focused images on the retina photoreceptors is a state of refraction called emmetropia. When a refractive error is present and the eye is unable to bring parallel light rays from a distant object into focus, the condition is referred to as ametropia [2]. There are three basic defocus conditions that may produce it: myopia, hyperopia and astigmatism [3]. All of these refractive errors are classified as low-order [4] or also called primary aberrations [5] and contribute around 90% to overall wave aberrations in the human eye [6]. Astigmatism, for example, is not a pathologic state but rather a defect result from the irregularities in the radius of curvature of the cornea, due to anatomy variations; most people have some degree of astigmatism [7,8].

Through a suitable refractive evaluation, these refractive errors can be corrected either with spectacles, contact lenses or refractive surgery. Nowadays a variety of instruments are available for the evaluation of the eye's refractive condition to assist eye care professionals. One of these devices is known as an ophthalmometer, a non-contact apparatus designed to measure the size of an image formed on the cornea (a convex reflecting surface), and from this data it calculates the curvature radii in the central part of the anterior corneal surface. The method of examining a patient's cornea with an ophthalmometer is called keratometry. Within the main goals of this procedure are: determining refractive power in diopters, location, magnitude, and direction of ocular astigmatism, assisting in the fitting of contact lenses, and in some cases measuring back optic zone curvature of contact lenses [9,10].

The ophthalmometer also called keratometer is restricted to measure the apical zone between 3–4 mm diameter depending upon corneal curvature [11]. These devices can be divided in two main groups: manual and automatic. Within the manual group are the Bausch & Lomb, Helmholtz–Littman, Javal–Schiotz, Haag–Streit, Chamber–Inskeep. The automatic ones are the optoelectronic automated keratometers [12]. Measurements with manual ophthalmometers are affected by nystagmoid movements, which is why most of them apply the doubling principle using prisms and can be subclassified in one and two position keratometers. The one position keratometer allows measuring two orthogonal meridians without rotating the instrument. Two position keratometers [13] require a 90° rotation to measure each meridian separately which makes it more sensitive to detect irregular astigmatism [14].

Ophthalmometers apply the approximated keratometer equation to estimate curvature radii of the cornea based on the image formation on a spherical convex mirror by paraxial optics. This method considers that the formed virtual image is placed at the focal plane of the mirror, but in reality, the distance between the object and where the virtual image actually forms is shorter than the distance between object and focal plane. For this reason, the measured curvature radii will be smaller than the real value. The inherent error can be up to 0.35% (0.03 mm) [15]. In this article, an exact equation is proposed along with a method that provides advantages over the instruments currently used.

2. Proposed method

2.1. Equation deduction

An object with height h is placed in front of a spherical mirror with a center of curvature C, forming a virtual image h', as shown in Fig. 1. The distance between vertex and object is given by l, and distance between vertex and virtual image by l'.

Considering, as shown in the literature [16-22], that the virtual image forms on focus, the radii of curvature can be calculated with the general approximated keratometer equation shown as follows:
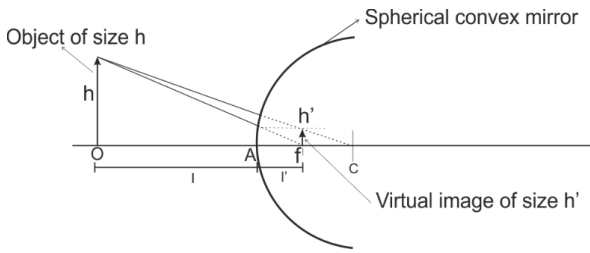
$$r = 2\,h'l/h \tag{1}$$

Fig. 1. Virtual image formation by a convex spherical mirror with image placed at focal plane.
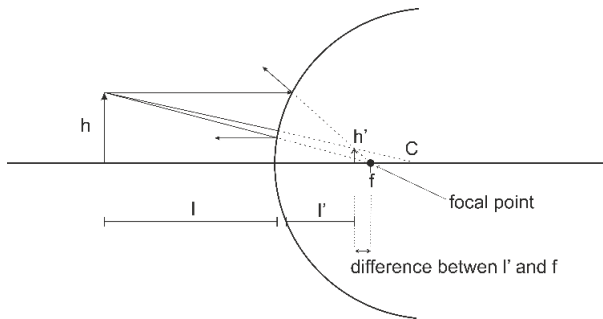

Fig. 2. Distance difference between focal plane and vertex to true place of virtual image formation.

However, there is a difference between the distance where the image actually forms and the focal length of the mirror as seen in Fig. 2.

The error produced by this difference can be reduced by increasing the object-to-image distance *l* or compensated by adding the error to the keratometry measurement [23,24]. Nevertheless, in order to minimize inaccuracies in a measurement system using Eq. (1), we propose an analysis based on the premise that light rays that form an image on a convex spherical mirror, follow a straight line as an optical path. It is possible to use equations on the straight lines that form the image and the point where it intersects to obtain an exact approximation of the radius of curvature of the spherical surface [25]. Following Fig. 3:
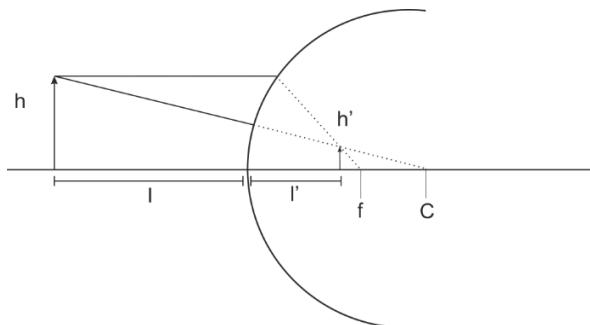

Fig. 3. Straight lines that form the virtual image.

Taking the (0, 0) coordinate as the mirror's vertex and $x_1 = -l$, $y_1 = h$, $x_2 = r$, and $y_2 = 0$:

$$m = \frac{-h}{r + l} \tag{2}$$

Straight line general equation is defined as $y = mx + b$ from which the slope m was obtained and $y = 0$, $x = r$:

$$0 = \frac{-h}{r + l} r + b \tag{3a}$$

$$b = \frac{h r}{r + l} \tag{3b}$$

straight-line equation for $(\overline{h r})$ is:

$$y = \frac{-h}{r + l} x + \frac{h r}{r + l} \tag{4}$$

similar analysis for $(\overline{h'f})$ being $x_1 = l'$, $y_1 = h'$, $x_2 = f = r/2$, and $y_2 = 0$:

$$m = \frac{-h}{r/2 - l'} = \frac{-2h'}{r - 2l'} \tag{5a}$$

$$0 = \frac{-2h'r}{r - 2l'} \frac{r}{2} \tag{5b}$$

$$b = \frac{h'r}{r - 2l'} \tag{5c}$$

$$y = \frac{-2h'}{r - 2l'} x + \frac{h'r}{r - 2l'} \tag{5d}$$

combining equations (4) and (5), we obtain

$$\frac{-h}{r + l} x + \frac{h r}{r + l} = \frac{-2h'}{r - 2l'} x + \frac{h'r}{r - 2l'} \tag{6}$$

intersection point between two straight lines occurs when $x = l'$:

$$\frac{-h l'}{r + l} + \frac{h r}{r + l} = \frac{-2h'l}{r - 2l'} + \frac{h'r}{r - 2l'} \tag{7}$$

applying the lateral magnification equation:

$$h'/h = l'/l \tag{8}$$

we get an exact equation for the radii of curvature:

$$r = -\frac{2h'l}{h - h'} \tag{9}$$

In the case of a convex mirror, distance *l* is negative; therefore, the equation has a negative sign. Equation (9) is function of the known object's height, virtual image's height, and distance from object to vertex, which are data that can be measured experimentally.

2.2. Proposed technique

For the practical implementation of the proposed method, we use a circular fringe cosine pattern as an equivalent mire of a keratometer [26] (which is continuous unlike those used in Placido systems that follow a binary profile [27]). This pattern was recorded in a black-and-white film (P) Kodak Tri-X pan TXT4164, through an LCD monitor LG MD2362D and a large format camera Linhof -Technika V. The pattern was generated with MATLab® following Eq. (10) and is shown in Fig. 4.

$$f(x^p, y^p) = a^p + b^p \cos(2\pi \cdot r(x_p, y_p)/R)^\gamma \tag{10}$$

The pattern recorded in the film is illuminated with a white LED luminescent panel (LS) 10×10 cm. Also, in order to emulate a healthy cornea, a calibration sphere (CS) of a NIDEK® Magellan Mapper corneal topographer with a nominal cur-
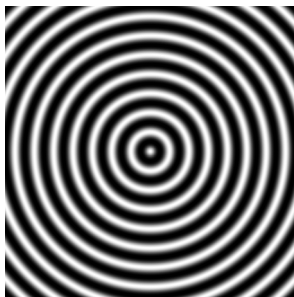

Fig. 4. Digital fringe cosine pattern with values a^p, $b^p = 128$, a gamma value $\gamma = 1.5$ and a radius value $R = 68$ pixels and (x_p, y_p) is the pixel coordinate of the LCD.
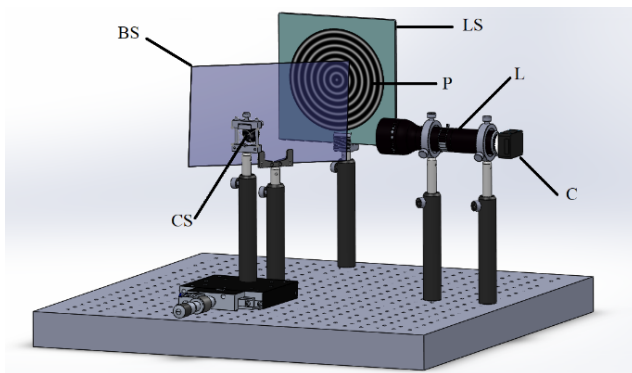

Fig. 5. Schematic of the proposed experimental set-up.

vature radius of 7.865 mm, was mounted in a micrometric one direction translation stage. The pattern forms a virtual, erect and diminished image and it is captured with a CCD camera (C) with 1.25 MP effective pixels, using a telecentric lens (L). To maintain orthogonality between illuminated pattern, sphere and cam, we use an optical beam splitter 40/60 (BS). A set up scheme is shown in Fig. 5. Images were captured by the camera and processed with LabVIEW™ and IMAQ Vision®.

2.3. Image analysis and data extraction

The main goal of the proposed technique is measuring the size of the virtual image and mire. Since the mire is a negative cosine pattern, there will be a maximum and minimum in all the contained periods; minima and maxima locations can be radially detected throughout 360°.

The pattern was spatially designed to contain a signal with fourteen extrema locations (not counting the center), where theoretically 5040 points can be analyzed. A radial line profile was performed, producing a signal with an amplitude range of 256 gray levels that correspond to the 8 bits pixel intensity of the experimental image. Basically, the radial line profile can be implemented to recover one dimensional signal for any particular interest angle.

A minima and maxima extraction algorithm based on persistence [28] was applied to the signals of interest. Once extrema locations have been found, (x, y) coordinates of each can be extracted from the image. Finally taking these coordinates (maxima marked in yellow circles in Fig. 6) and with the pattern center coordinate (k, b), the Pythagorean theorem can be applied to each triangle formed by these points using the following equation:

$$(x - b)^2 + (y - k)^2 = r^2 \tag{11}$$

Knowing h, h' size for each maximum and minimum points, all parameters of Eq. (9) are known and the radius of curvature is calculated for each max and min points.
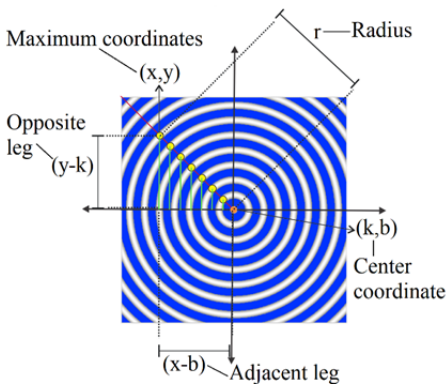

Fig. 6. Scheme to calculate h and h' through the Pythagorean theorem.

3. Experimental setup

3.1. Image analysis and data extraction

Taking into account the nominal radius of curvature of the test sphere, the mire was placed at a distance $l = 130$ mm following the equations of image formation in a convex mirror [29] to obtain a virtual image height of 1.5 mm, and therefore analyze a circular area with 3 mm diameter. Distance between lens and calibration sphere is equal to the nominal working distance (WD) of the lens 173 mm. It can be displaced with the micrometric translation stage, to adjust the location of the sphere until a horizontal field of view of 9.6 mm is reached, which is established by the manufacturer at the WD [30], ensuring that the components were at the proposed distances. Figure 7**a** shows experimental setup from a top view and all distances are shown in Fig. 7**b**. The mire image was captured by a f 18 mm double Gauss lens and the same cam.
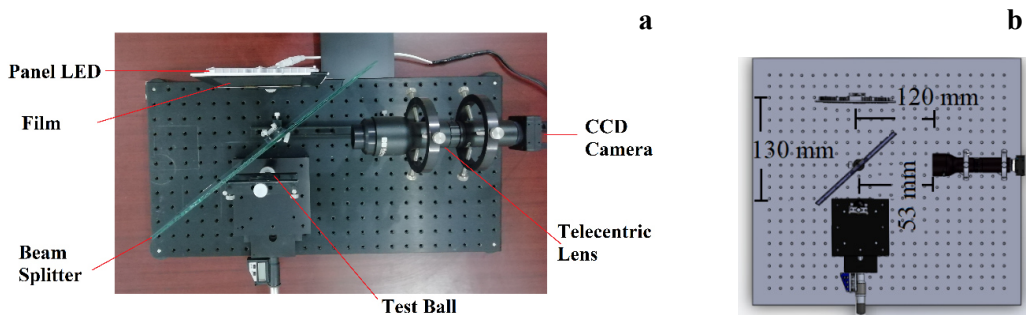

Fig. 7. (**a**) Experimental setup top view, (**b**) distance between components.

3.2. Diopters and ophthalmic measurements

In optometric practice, eye care professionals like optometrists or opticians often are more related with keratometric diopters (D), instead of curvature radius. To calculate dioptric power, Eq. (12) should be applied [31], using an index of refraction $n_2 = 1.3375$ which is the value used with most keratometers [32].

$$D = \frac{n_2 - n_1 (1000 \text{ nm/m})}{r} \tag{12}$$

When the refractive power of a cornea is identical in all meridians, it can be considered as a perfect spherical. In regular toric corneas there are two perpendicular meridians with the highest or lowest refractive power [33]. These are called primary (180°) and secondary (90°). Within types of astigmatism are "with the rule" (WTR) which occurs when the flattest corneal meridian is lying near the primary one, and "against the rule" (ATR) which is when the flattest meridian is along the secondary one. There is also oblique astigmatism and it occurs when the principal meridians are from 30° to 60° and 120° to 150° [34]. The last case is the irregular astigmatism, in which the

principal meridians of the cornea are not perpendicular to one another [35]; and in its presence, mire pattern images will be distorted [36].

We performed measurements along these principal meridians, and at the ones lying at 45° and 135° as possible locations in the cases of oblique astigmatism. However, since it is a pattern with radial symmetry, there is a possibility of making a line profile at any angle on the pattern of the captured virtual image. Two images were used and 52 measurements taken in order to compute the statistical parameters in a representative sample.

4. Experimental results

4.1. Object and virtual image signals

The variables h and h' in Eq. (1) were obtained from the object and virtual images, presented in Fig. 8.

A Gaussian smoothing filter with a kernel size of 5 was applied to the captured image for de-noising and to eliminate small abrupt transitions in the gray scale values, which affected the minimum location. The kernel values are specified in Fig. 9.

Figures 10 and 11 show signals corresponding to the object and virtual image from primary meridian and their respective max and min locations. The abscissa axis represents the analyzed diameter (analyzed meridian distance).
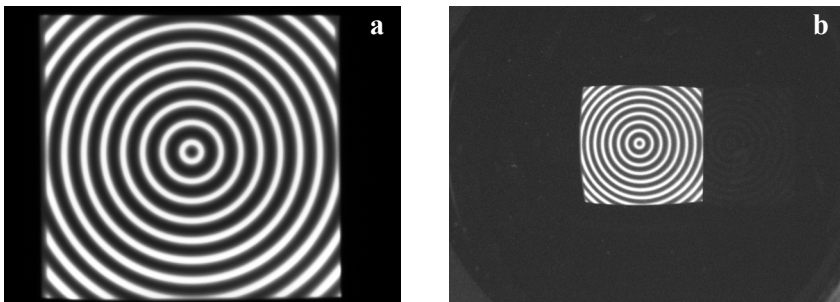

Fig. 8. (**a**) Gray scale image captured of the pattern, (**b**) gray scale image captured of virtual image on the test sphere.

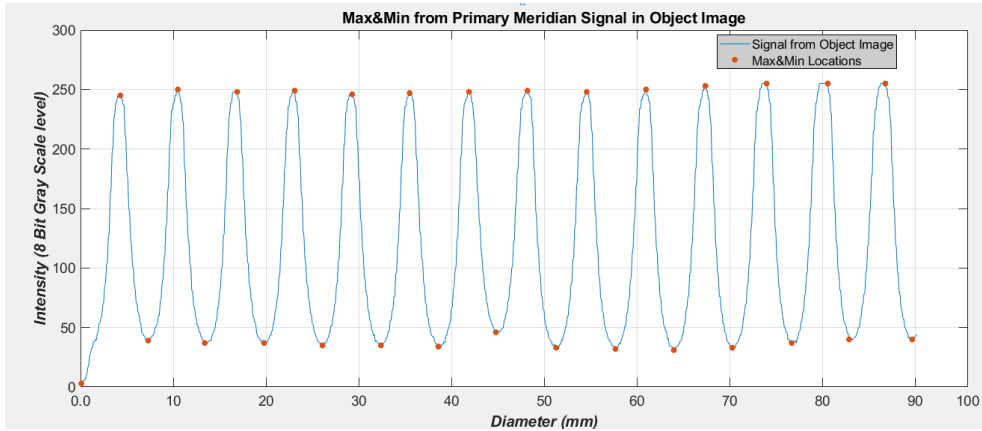Fig. 9. Gaussian smoothing filter kernel values.

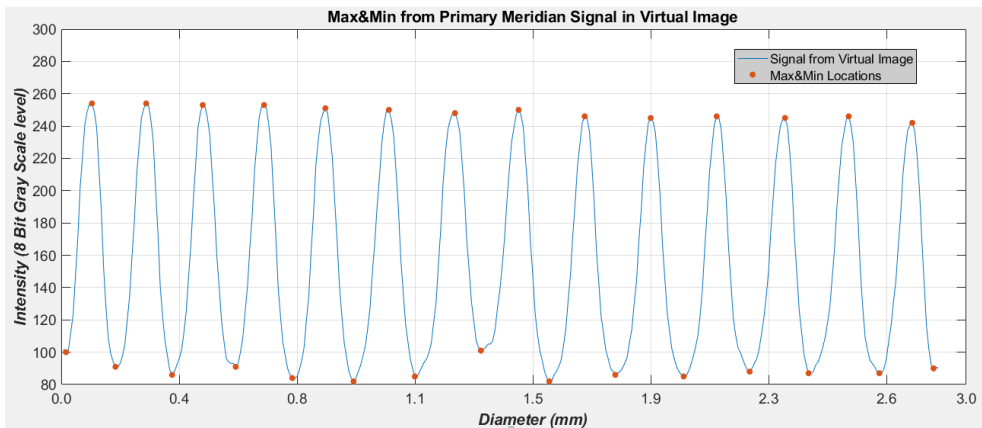Fig. 10. Max & min locations in red points from object signal.

Fig. 11. Max & min locations in red points from virtual image signal.

4.2. Measurements results with test sphere

Using the signals corresponding to the four meridians (primary, secondary, and ob-liques), the radii of curvature was obtained for each pair of heights found h, h'. Since measurements obtained first-hand (raw data) were out of tolerance according to ISO10343 [38], it was necessary to perform a linear fit by least squares method to each data set, to compensate the measurements according to the general line:

$$R_{\text{adj}} = mR_{\text{meas}} + b \tag{13}$$

where R_{adj} is the adjusted power value, R_{meas} is the measured radii of curvature, m is the slope of a straight line, and b is the intersection point. The values obtained for the
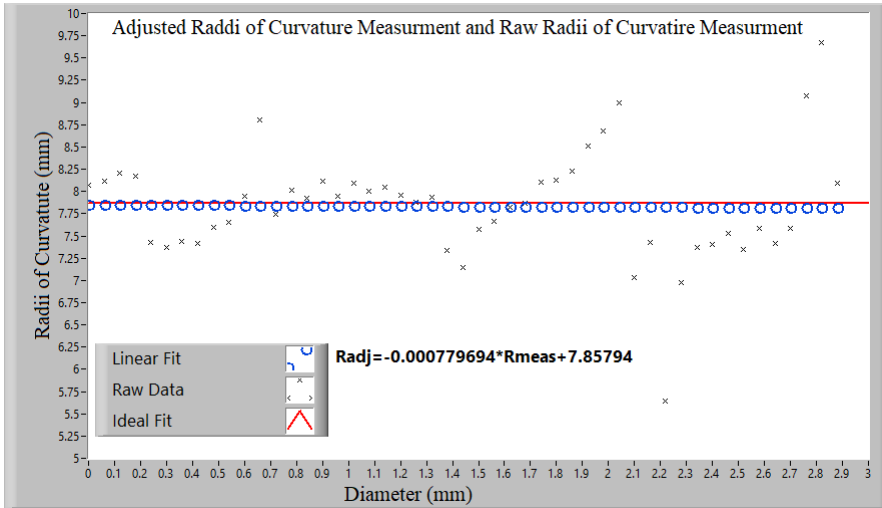
Fig. 12. Black crosses represent raw measurements, the blue circles data are fitted and the red line an ideal linear fit to the measurements in the primary meridian.

T a b l e 1. Compensate statistics values computed with the exact proposed equation (9).

Meridian	RMS [mm]	RMS Err [mm]	Mean [mm]	Mean Err [mm]	Diopters D	Diopters Err	2σ [mm]
			Statistics parameters				
180°	7.8384	0.0311301	7.83845	0.026593	43.0573	0.1721	0.03
90°	7.8573	0.0139087	7.85735	0.011515	42.9536	0.0769	0.02
45°	7.8484	0.0298887	7.8484	0.024724	43.003	0.1648	0.03
135°	7.8176	0.0511061	7.81758	0.047423	43.1723	0.2825	0.05

primary meridian are: $m = -0.00077$ and $b = 7.85794$. In Fig. 12, the linear fit, raw data and ideal linear fit can be visualized.

A total of fifty-two error values were used to calculate the accuracy and precision of the proposed method. Other parameters as: root mean square (RMS) Eq. (14) [37], root mean square error (RMS Err) Eq. (16), mean Eq. (15), mean error Eq. (17) and standard deviation were also determined. The ISO 10343 [38] standard establishes twice the standard deviation as the accuracy ±0.05 mm. The main statistic values are presented in Table 1. In all principal meridians, the adjusted measurements error values are within ISO10343.

$$\text{RMS} = \sqrt{\frac{1}{n}\sum_{i=0}^{n-1}|x_i|^2} \tag{14}$$

$$\text{RMS Err} = \sqrt{\sum_{i=1}^{n}\frac{1}{n}(x_i - \hat{x}_i)^2} \tag{15}$$

$$\text{Mean} = \frac{1}{n} \sum_{i=0}^{n-1} x_i \tag{16}$$

$$\text{Mean Err} = \sum_{i=1}^{n} \frac{1}{n} (x_i - \hat{x}_i) \tag{17}$$

$$\text{Std dev} = \sum_{i=0}^{n-1} \frac{1}{n} (x_i - \text{Mean})^2 \tag{18}$$

where x_i are the values of adjusted curvature radii and $\hat{x}_i$ is the nominal true value of the test sphere and n in the number of samples.

As can be seen in Fig. 12, most of the adjusted data represented by the blue circles are below the ideal adjustment (nominal radius of curvature of the sphere). This occurred in the other analyzed meridians, therefore, the mean values presented in Table 1 are less than the nominal value. Figure 13 shows an error graph obtained after measurement compensation in the primary meridian.
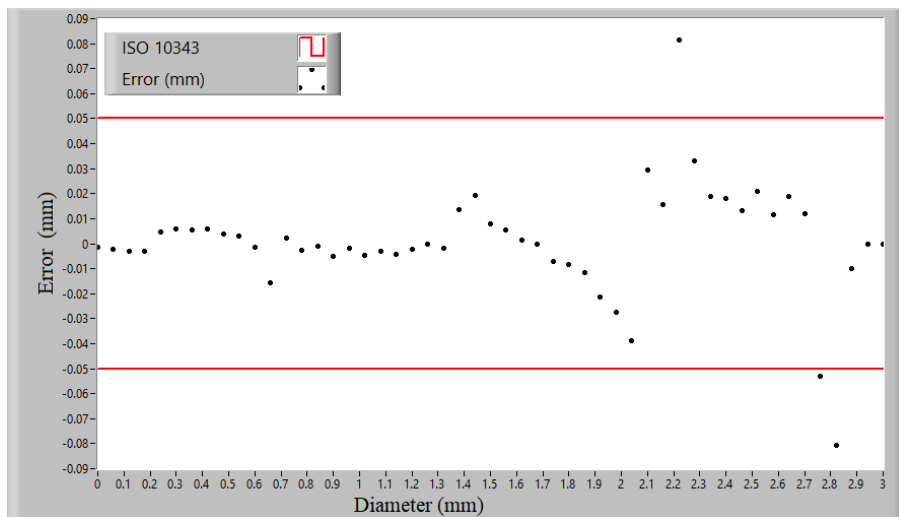

Fig. 13. Obtained result error for adjusted radii of curvature in the primary meridian.

In order to verify the effectiveness of the proposed equation, the same procedure was carried out applying the approximate equation of the keratometer (Eq. (1)). This equation does not contain the subtraction of the height of the virtual image from the object height. Equation (1) gives values of radius of curvature smaller than it should be, therefore, the error in the mean of each meridian is larger than those presented in Table 1 where the results were obtained using the exact Eq. (9).

A summary of the statistical values obtained is shown in Table 2.

T a b l e 2. Compensate statistics values computed by approximated keratometer equation (1).

Meridian	RMS [mm]	RMSE [mm]	Mean [mm]	Mean Err [mm]	Diopters D	Diopters Err	2σ [mm]
			Statistics parameters				
180°	7.64688	0.227213	7.64662	0.21838	44.1416	1.28233	0.44
90°	7.62154	0.245705	7.62147	0.24353	44.284	1.38662	0.49
45°	7.6113	0.25432	7.61128	0.25372	44.3424	1.43592	0.43
135°	7.5834	0.282156	7.58338	0.28161	44.5055	1.59872	0.56

It is evident that the values obtained by computing the results with the approximate equation are outside the tolerance of the standard ISO 10343, leading to errors above 1%.

5. Conclusions

A method to measure radius of curvature in a calibration sphere, based on an exact equation, was presented. The experimental setup consists of a few elements that are generally affordable. Basically, the proposed method only requires two images, one of the circular fringe pattern mire and the virtual image formed by specular reflection on the test sphere. From these two pictures, a software developed in LabVIEW® obtains a line profile of the principal meridians, thus extracting four signals. An extrema detection algorithm is applied, where their position (x, y) coordinates are obtained, and through the Pythagorean theorem object size h and virtual image size h' are calculated.

Substituting values of h' and h in Eq. (9) and using the known distance l from the calibration sphere to the pattern, the radius of curvature was calculated. After data compensation, the proposed formula and experimental setup were used under the limits marked by ISO 10343. Since the pattern displayed is a cosine, there is a possibility of performing a radial analysis; in addition, the pattern will be modulated by the presence of any kind of aberration, being able to detect and locate regular or irregular astigmatism without the need to adjust the mire as in manual keratometers. The implemented algorithm has such low computing time that the software could be used in a real application or for commercial use.

Some improvements can be implemented in the system, such as an automated alignment using motorized translation stages instead of manual ones, along with a high-resolution camera. Further investigation and experimental setup changes are contemplated for future work to carry out measurements of corneas *in vivo*. One of the main changes to be made is the implementation of an automatic system for aligning the center of the pattern with respect to the vertex of the cornea using a head positioning fixture complemented by an optimal fixation target controlled with a (x, y, z) scroll mount to move the pattern. To take into account the effects of asphericity, toricity and spherical aberration of the real corneas, a frequency modulation of the cosine pattern will be developed in order to maintain same rings size outside the central corneal zone. In addition, a compensation using a null test approach should be made. The implemented algorithm

has such low computing time that the software could be used in a real application for commercial use.

References

[1] REMINGTON L.A., *Clinical Anatomy and Physiology of the Visual System*, 3th Ed., Elsevier Butterworth-Heinemann, St. Louis, Missouri 2012, p. 21.

[2] SCHWIEGERLING J., *Field Guide to Visual and Ophthalmic Optics*, SPIE Press, Bellingham, Washington 2004, p. 23.

[3] BLOMQUIST P.H., *Practical Ophthalmology: A Manual for Beginning Residents*, 7th ed., American Academy of Ophthalmology, San Francisco, CA, 2015, p. 53.

[4] SKUTA G.L., CANTOR L.B., WEISS J.S., *Basic and Clinical Science Course, Section 13: Refractive Surgery*, American Academy of Ophthalmology, San Francisco, CA, 2012, p. 146.

[5] YANOFF M., DUKER J.S., *Ophthalmology*, 3th Ed., Elsevier, New York, 2009, p. 53.

[6] LOMBARDO M., LOMBARDO G., *Wave aberration of human eyes and new descriptors of image optical quality and visual performance*, Journal of Cataract & Refractive Surgery **36**(2), 2010, pp. 313–331, DOI: 10.1016/j.jcrs.2009.09.026.

[7] DAVIDOVITS P., *Physics in Biology and Medicine*, 4th Ed., Academic Press, Burlington, MA, USA, 2013, pp.227.

[8] YANOFF M., CAMERON D., *Goldmans CECIL Medicine*, 24th Ed., Elsevier Saunders, Philadelphia, PA, 2013, p. 2428.

[9] GASSON A., MORRIS J.A., *The Contact Lens Manual: A Practical Guide to Fitting*, 4th Ed., Butterworth-Heinemann, Oxford, UK, 2010, p. 23.

[10] EFRON N., *Contact Lens Practice*, 2nd Ed., Elsevier Health Sciences, New York, 2010, pp. 99–108.

[11] FRY L., GARG A., GUTIÉRREZ F., PANDEY S., TABIN G., *Clinical Practice in Small Incision Cataract Surgery*, Taylor & Francis, Boca Raton, FL., 2004, p. 310.

[12] KASHKE M., DONNERHACKE K.-H., STEFAN M., *Optical Devices in Ophthalmology and Optometry: Technology, Design Principles, and Clinical Applications*, 1st Ed., Wiley-VCH Verlag GmbH & Co. KGaA, Weinheim, Germany, 2014, pp. 147–276.

[13] SCHMIDTMANN G., *Clinical Vision Science a Concise Guide to Numbers, Laws and Formulas*, 1st Ed., Springer, Cham, Switzerland, 2020, pp. 132–136.

[14] BIKAS BHATTACHARYYA, *Textbook of Visual Science and Clinical Optometry*, 1st Ed., Jaypee Brothers, Medical Publishers, New Delhi, India, 2009, pp. 265–266.

[15] BENJAMIN W.J., *Borish's Clinical Refraction*, 2nd Ed., Elsevier Health Sciences, St. Louis, Missouri, USA, 2006, p. 647.

[16] ROSENFIELD M., LOGAN N., *Optometry: Science, Techniques and Clinical Management*, 2nd Ed., Elsevier Health Sciences, New York, USA 2009, pp. 257–276.

[17] KEIRL A., CHRISTIE C., *Clinical Optics and Refraction: A Guide for Optometrists, Contact Lens Opticians and Dispensing Opticians*, 1st Ed., Elsevier Health Sciences, Philadelphia, PA, 2007, pp. 187–189.

[18] ELKINGTON R., FRANK J., GREANEY J., *Clinical Optics*, 3th Ed., Wiley 1999, pp. 188–190.

[19] SKUTA G.L., CANTOR L.B., WEISS J.S., *Basic and Clinical Science Course, Section 3: Clinical Optics*, American Academy of Ophthalmology, San Francisco, CA, 2012, pp. 263–264.

[20] PHILLIPS A.J., SPEEDWELL L., *Contact Lens*, 6th Ed., Elsevier Health Sciences, St. Louis, Missouri, USA, 2019, pp. 158–173.

[21] ARTAL P., *Handbook of Visual Optics, Vol 1: Fundamentals and Eye Optics*, CRC Press, Boca Raton, FL, 2017, pp. 103–120.

[22] SMITH G., ATCHISON D., *The Eye and Visual Optical Instruments*, 1st Ed., Cambridge University Press, Cambridge, UK, 1997, pp. 245–269.

[23] Carlson N., Kurtz D., *Clinical Procedures for Ocular Examination*, 4th Ed., Mc. Graw Will Education, New York, 2015, pp. 401–402.

[24] Douthwaite W.A., *Contact Lens Optics and Lens Design*, 3rd Ed., Butterworth-Heinemann, Oxford, UK, 2006, p. 129.

[25] Mendoza-Villegas P.G., Trujillo-Schiaffino G., Salas-Peimbert D.P., Bustillos-Trujillo A., *Method of analysis to measure the tangential curvature in a test sphere*, Proceedings of SPIE **7499**, 2009, article 74990K, DOI: 10.1117/12.848966.

[26] Millodot M., *Dictionary of Optometry and Visual Science*, 7th Ed., Elsevier Health Sciences, New York, 2014, p. 229.

[27] Servín M., Quiroga J.A., Moisés Padilla J., *Fringe Pattern Analysis for Optical Metrology: Theory, Algorithms, and Applications*, 1st Ed., Wiley-VCH Verlag GmbH & Co. KGaA, Weinheim, Germany, 2014, p. 5.

[28] Kozlov Y., Weinkauf T., *Extracting and Filtering Minima and Maxima of 1D Functions*, 2012, [https://www.csc.kth.se/~weinkauf/notes/persistence1d.html] (accessed October 15, 2020).

[29] Dereniak E., Dereniak T., *Geometrical and Trigonometric Optics*, 1st Ed., Cambridge University Press, Cambridge, UK, 2008, pp. 193-225.

[30] #62-932 Telecentric Lens Data Sheet, Edmund Optics (2014). [https://www.edmundoptics.com/p/05x-23-c-mount-platinumtltrade-telecentric-lens/17562/].

[31] Smolin G., Stephen C., Azar D.T., Dohlman C.H., *Smolin and Thoft's The Cornea: Scientific Foundations and Clinical Practice*, 4th Ed., Lippincott Williams & Wilkins, Philadelphia, PA, 2005, pp. 169–174.

[32] Keating M.P., *Geometrical, Physical, and Visual Optics*, 2nd Ed., Butterworth-Heinemann, Woburn, MA, 2002, p. 105.

[33] Spaeth G., Danesh-Meyer H., Goldberg I., Kampik A., *Ophthalmic Surgery Principles and Practice*, 4th Ed., Elsevier Saunders, New York, 2012, pp. 179–181.

[34] Grosvenor T.P., *Primary Care Optometry*, 5th Ed., Elsevier Health Sciences, St. Louis Missouri, 2007, pp. 184–188.

[35] Wilkinson M.E., Shaid K.S., *Optics Review, Online Resource*, Iowa City, IA: Eye Rounds, University of Iowa, 2017, p. 42.

[36] Brightbill F.S., *Corneal Surgery: Theory, Technique and Tissue*, 4th Ed., MOSBY Elsevier, 2009, pp. 71–73.

[37] Freedman D., Pisani R., Purves R., *Statistics*, 4th Ed., W.W. Norton & Company, London, UK, 2007, p. 66.

[38] International Standard ISO, *10343:2014(E) Ophthalmic instruments – Ophthalmometers*, Geneva, Switzerland, (2014). [https://www.iso.org/standard/59705.html].